

# Electronic correlation in nearly free electron metals with beyond-DFT methods

Subhasish Mandal,<sup>1</sup> Kristjan Haule,<sup>1</sup> Karin M. Rabe,<sup>1</sup> and David Vanderbilt<sup>1</sup>

<sup>1</sup>*Department of Physics and Astronomy, Rutgers University, Piscataway, USA*

For more than three decades, nearly free electron elemental metals have been a topic of debate because the computed bandwidths are significantly wider in the local density approximation to density-functional theory (DFT) than indicated by angle-resolved photoemission experiments. Here, we systematically investigate this using first-principles calculations for alkali and alkaline-earth metals using DFT and various beyond-DFT methods such as meta-GGA,  $G_0W_0$ , B3LYP, and DFT+eDMFT. We find that the static non-local exchange and correlation, as partly included in the B3LYP hybrid functional, significantly increase the bandwidths even compared to LDA, while the  $G_0W_0$  bands are only slightly narrower than in LDA. The agreement with the ARPES is best when the local approximation to the self-energy is used in the DFT+eDMFT method. We infer that even moderately correlated systems with partially occupied  $s$  orbitals, which were assumed to approximate the uniform electron gas, are very well described in terms of short-range dynamical correlations that are only local to an atom.

The alkali and alkaline-earth metals, whose electronic structure has been studied since the inception of quantum mechanics [1], are often assumed to be the closest natural analogs to the uniform electron gas (UEG). Density functional theory (DFT) in the local density approximation (LDA), which connects each point in space inside a crystal to a uniform electron-gas problem through the electron density, is found to be fairly successful in the qualitative description of these metals, making them exemplary systems for weakly correlated electrons. However, the excited-state spectra and consequently the occupied bandwidth often quantitatively disagree with angle-resolved photoemission spectroscopy (ARPES) experiments. For example, ARPES studies by Lyo and Plummer [2] indicates that the bandwidth of the first occupied band of sodium is substantially narrower than predicted by LDA. This has triggered a large amount of experimental [3–8] and theoretical [9–21] work over the last three decades.

An earlier study using the  $G_0W_0$  approximation [22], which truncates the self-energy to first order in the Green's function  $G_0$  and the screened Coulomb interaction  $W_0$ , pointed to the importance of many-body effects, suggesting that the lowest-order perturbative term may not be sufficient to describe the excitation spectrum in these materials [10]. This motivated further GW studies to include higher-order perturbative corrections to the band limit [20, 21, 23, 24]. Mohan and Sernelius [9] and more recently Kuteepov [17] found that the inclusion of vertex corrections (GWT) modifies the GW self-energy, but the low-order vertex corrections to the self-energy and the dielectric function nearly cancel each other, resulting in a bandwidth renormalization not very different from the  $G_0W_0$  prediction.

Recent work using a sophisticated unbiased reptation Monte Carlo method further indicates that the vertex corrections and self-consistency aspects of GW cancel to a large degree near the Fermi surface [25]. This result also hints that the elemental metallic systems might be moderately correlated. An opposite trend of increasing the bandwidth compared to LDA is found in recent

studies using self-consistent GW [20, 23] and variational and fixed-node diffusion quantum Monte Carlo [26] techniques. Contrary to the indications from the GW approximation, Zhu and Overhauser [27] predicted that the spin fluctuations within a paramagnon pole model could account for the bandwidth reduction in Na, but a more recent study [19] found that this effect is negligible. This controversy remains unresolved, and the reason for the discrepancies between ARPES measurements and the theoretically predicted bandwidths in these simple metals remains one of the fundamental questions in condensed matter physics.

On a different tack, the narrowing of the ARPES spectra has alternatively been ascribed to final-state effects, which would require treating the outgoing electron as embedded in an interacting uniform electron gas inside the solid, rather than as a free electron leaving the solid [20]. A similar approach was taken in Refs. [28] and [10], but with the inclusion of surface effects. Such an interpretation was challenged in Ref. [11] (see also [21]), as it would invalidate the accepted interpretation of the ARPES experiments as measuring the single-particle spectral function weighted by matrix-element effects [29]. This would have far-reaching implications for the interpretation of all ARPES data to date.

Several “beyond-DFT” methods have been developed over the past decades to describe correlated systems. These are often applied to open-shell  $d$ -electron systems, where the corrections to DFT are large and often qualitative, but very little is known about the applicability of these methods to solids that are only moderately correlated. In particular, the DFT+eDMFT method, which has gained wide popularity for describing the electronic structure of localized  $d$ - and  $f$ -electron systems, has so far mainly been applied to study strongly correlated systems [30–41], while its extension to the weak coupling limit is rarely discussed in the literature.

Here we systematically apply DFT and beyond-DFT methods to the elemental metallic systems from the first and second columns of the periodic table (Li to Cs and Be to Sr), and show how the effects of local and non-

local exchange and correlations impact the bandwidth and band structure. We find that the band narrowing is surprisingly well described with non-perturbative dynamical correlations modeled as local to an atom rather than to a point in 3D space, emphasizing the importance of umklapp contributions to the electron self-energy. In particular, in this letter we show that the elemental metals with partially occupied *s* orbitals, which are usually assumed to be nearly-free-electron metals, are in fact moderately correlated, thus forcing a reconsideration of long-held notions about these simple metals.

*Method and Structural Details:* All computations are performed for the room-temperature experimental crystal structures obtained from the ICSD database. Most of the elemental metals studied here crystallize in the bcc structure at room temperature, except for Be and Mg which crystallize in hcp, and Ca and Sr in fcc.

We compute band structures for Li, Be, Na, Mg, K, Ca, Rb, Sr, and Cs using DFT (LDA and PBE) and beyond-DFT methods, including the modified Becke–Johnson (mBJ) meta-GGA potential; the B3LYP hybrid functional;  $G_0W_0$ ; and DFT+DMFT with embedded-DMFT (eDMFT). The computed values of  $U$  for the metallic systems using the self-consistent constrained-eDMFT method are all found to be close to  $U = 5$  eV, a value which we adopt for all the compounds studied here (see the S.I.). Thus,  $U$  is not treated as a tuning parameter. The DFT parts of all the methods used here are performed with the all-electron WIEN2K [42] LAPW package using a consistent basis and parameter set, thus allowing for direct comparisons of the effects of long- and short-range correlations and the elucidation of their static and dynamic nature.

We also compute the  $G_0W_0$  bands, which is challenging for metallic systems due to numerical difficulties associated with the treatment of the Fermi surface singularity, often leading to less accurate results on the Matsubara axis, and consequently, extreme difficulty in the analytic continuation to real frequencies. This has been discussed in detail in Ref. [43], where the algorithm for the frequency convolution on the Matsubara axis was improved. This allows a stable analytic continuation of the imaginary-axis data via a Pade approximation, which is carried out for GW band structure calculations throughout the Brillouin zone (BZ).

*Results:* In the following we compare the electronic band structures using the above-mentioned methods with ARPES data, which are available for Na, K, and Mg. We describe each of these compounds in detail here, and direct the reader to the S.I. for the others.

*Sodium:* We first describe our results for Na, which has been most widely discussed in the literature as a prototypical UEG elemental metal. The computed band structures in LDA, mBJ, B3LYP,  $G_0W_0$ , and eDMFT are shown in Fig. 1. We directly compare with the ARPES data (shown in pink dots), which are adopted

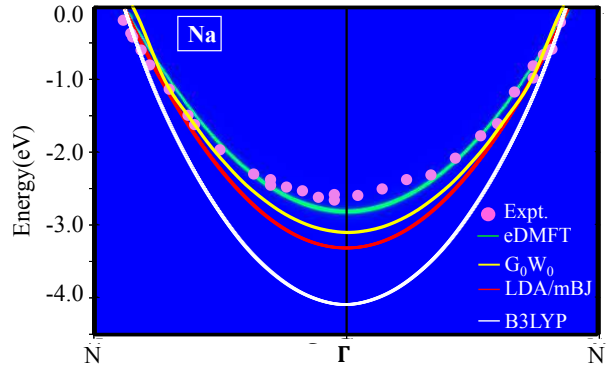


FIG. 1. (Color online) Band structure of elemental Na as computed in LDA, mBJ,  $G_0W_0$ , B3LYP, and eDMFT. Pink dots indicate angle-resolved-photoemission(ARPES) data from Ref. [2].

from Ref. [44]. Since the LDA and mBJ bands are found to be almost identical, we only show the LDA bands in the figure. While the bands are very similar to each other close to the Fermi surface at the  $N$ -point for all the methods, the differences between them become more evident near the  $\Gamma$  point.

Among these methods, the discrepancy between the B3LYP bands and the experiment is large. The agreement with ARPES for simple LDA is substantially better than for B3LYP. We also compute the  $G_0W_0$  bands, which is challenging for metallic systems due to numerical difficulties associated with the treatment of the Fermi surface singularity, often leading to less accurate results on the Matsubara axis, and consequently, extreme difficulty in the analytic continuation to real frequencies. This has been discussed in detail in Ref. [43], where the algorithm for the frequency convolution on the Matsubara axis was improved. This allows a stable analytic continuation of the imaginary-axis data via a Pade approximation, which is carried out for GW band structure calculations throughout the Brillouin zone (BZ).

It is evident in Fig. 1 that the  $G_0W_0$  band (yellow) is very close to the LDA bands, narrowing only slightly relative to the LDA even at the  $\Gamma$ -point. The agreement between theory and experiment is best for the eDMFT method; the spectral function (green) reproduces the ARPES data well throughout the BZ, except near the  $\Gamma$  point where the agreement is slightly worse.

*Potassium:* We perform similar comparisons for bcc K in Fig. 2, where we plot the band structures as computed in LDA, mBJ, B3LYP,  $G_0W_0$ , and eDMFT. The ARPES data (shown in pink dots) are taken from Ref. [44]. For K, the ARPES data are not available for the entire BZ, extending only about halfway from  $\Gamma$  to  $N$ . We again see that the bands obtained using various methods cross the Fermi energy at almost the same  $k$  point, but the dispersion towards  $\Gamma$  is quite different for the various methods.

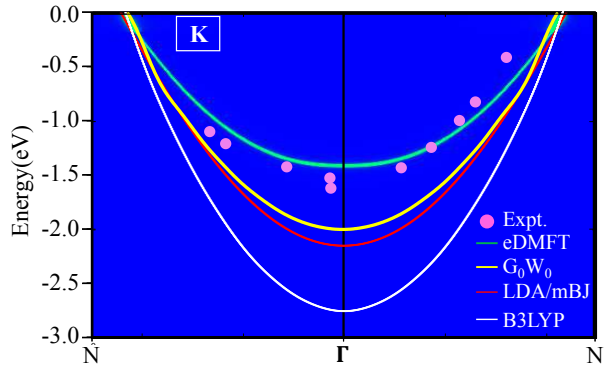


FIG. 2. (Color online) Band structure of elemental K as computed in LDA, mBJ,  $G_0W_0$ , B3LYP, and eDMFT. Pink dots indicate angle-resolved-photoemission(ARPES) data from Ref. [5].

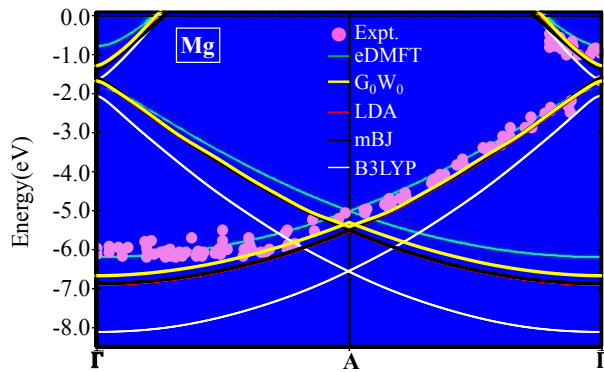


FIG. 3. (Color online) Band structure of elemental Mg as computed in LDA, mBJ,  $G_0W_0$ , B3LYP, and eDMFT. Pink dots indicate angle-resolved-photoemission(ARPES) data which are adopted from Ref[4].

The B3LYP band disperses the most, reaching  $-2.76\text{ eV}$  at  $\Gamma$ , while LDA and mBJ disperse only to  $-2.15\text{ eV}$ . As was the case for Na, the LDA and mBJ bands are almost indistinguishable, so we display only the LDA in Fig. 2. The  $G_0W_0$  bands narrow only slightly, reducing the bandwidth to  $2.00\text{ eV}$  from the LDA value of  $2.15\text{ eV}$ . The eDMFT narrows the bandwidth to  $1.42\text{ eV}$  at  $\Gamma$ , as compared with the experimental value of  $1.6\text{ eV}$ . (Slightly away from  $\Gamma$ , the ARPES data are asymmetric due to inaccuracy in the experimental data. As a result, the eDMFT band crosses the ARPES band only on the right half of the figure. A similar artifact appears for Na in Fig. 1.)

*Magnesium:* Unlike most of the elemental metals, Mg crystallizes in the hcp instead of the bcc structure at room temperature and has multiple occupied bands. We display the bands in Fig. 3. The ARPES data (pink dots, taken from Ref. [4]) indicate two bands within this energy range, one with small and one with large dispersion from the Fermi energy to  $\Gamma$ . In particular, one band disperses

Compound	LDA	mBJ	B3LYP	eDMFT	$G_0W_0$	Expt
Li	3.46	3.30	4.41	2.60	3.39	
Be	4.28	4.25	5.05	4.41	4.48	4.8 [3]
	11.03	10.90	12.73	10.12	11.37	11.1 [3]
Na	3.30	3.29	4.09	2.84	3.15	2.65 [44]
Mg	1.31	1.35	8.09	6.18	6.66	6.15 [4]
	1.65	1.61	2.07	1.85	1.68	1.70 [4]
	6.89	6.89	8.09	6.18	6.66	6.15 [4]
K	2.15	2.13	2.76	1.42	2.00	1.60 [5]
Ca	3.98	3.82	4.88	3.24	3.79	3.30 [6]
Rb	1.99	1.96	2.53	1.81	1.86	
Sr	3.7	3.48	4.46	3.05	3.39	
Cs	2.15	1.95	2.60	1.70	2.00	

TABLE I. Bandwidth of occupied bands for various elemental metals as computed in various beyond-DFT approaches.

from  $\Gamma$  at  $-0.82\text{ eV}$  up to the Fermi energy ( $E = 0$ ), and another disperses from  $-1.85\text{ eV}$  down to  $-6.15\text{ eV}$  along  $\Gamma$ -A- $\Gamma$ . Here we also find a similar trend in the computed bands using various methods as noticed for Na and K. The B3LYP bands disperse the most and lie furthest from the experimental bands. Once again, the LDA and mBJ bands are both very similar. The first  $G_0W_0$  band disperses to  $-1.29\text{ eV}$  at  $\Gamma$ , while in eDMFT it is  $-0.82\text{ eV}$  and in the experiment, it is  $-0.9\text{ eV}$ . The second occupied band crosses the  $\Gamma$  at  $-6.66$ ,  $-6.18$ , and  $-6.15\text{ eV}$  in  $G_0W_0$ , eDMFT, and experiment, respectively. We again find the best overall agreement with ARPES for the eDMFT spectral function. We find similar trends in the band structures of other elemental metals in this family as well, as discussed in the Supplement.

*Bandwidth of elemental metals:* To quantify the observed trends in alkali and alkaline-earth metals, we compare the bandwidths of the occupied bands, defined as the depth of the energy at  $\Gamma$  below  $E_F$ , as computed using LDA, mBJ, B3LYP,  $G_0W_0$ , and eDMFT, in Table I.

We also compare them with available experiments from ARPES as well as other photoemission spectroscopies. As the Fermi surface is almost exactly spherical in these compounds, and the band structure is close to a renormalized free-electron solution in the proper periodic potential, the most relevant number here is the bandwidth. LDA overestimates the bandwidths across the family as expected, except for Be. The hybrid functional, which corrects most of the self-interaction error by incorporating a fraction of exact exchange,

correcting the non-local part of the self-energy, has been found to significantly improve the descriptions of many *d*-electron systems [45–49]. Here we find that the non-local corrections included in B3LYP have the opposite effect, worsening the comparison with ARPES as it significantly overestimates the bandwidth for all the systems studied here. This clearly shows that the hybrid functionals do not improve on DFT for metallic systems [50]. mBJ performs better than B3LYP and gives very similar bandwidths as LDA, except for heavy elements such as Sr and Cs, where mBJ performs better than LDA. Next, we notice that the bandwidths as computed in the  $G_0W_0$  method are in better agreement than LDA or mBJ, but are still substantially narrower than those measured by ARPES. Various implementations of the GW approximation, with and without vertex corrections, give the bandwidth for Na in the range of 2.5–3.2 eV [18, 51]. Here we obtain 3.15 eV, quite similar to recently reported self-consistent quasiparticle GW values of 3.17 eV [51]. The improvement of GW as compared to static hybrid methods, which incorporate some Hartree-Fock self-energy, shows that the dynamical nature of the exchange and correlation is certainly an important factor in the band narrowing in Na and other alkali metals.

Finally, the bandwidth narrowing is even stronger in eDMFT due to the dynamic correlations incorporated in the strong frequency dependence of the self-energy, which substantially improves the agreement with ARPES experiments. While within DFT+*U*, the static analog of DFT+eDMFT, the bandwidth is insensitive to the value of *U* (not shown here), in the DFT+eDMFT results here, the bandwidth does depend on the local Coulomb interaction value *U* (see the S.I.). It is intriguing to understand why the bands in LDA and  $G_0W_0$  have almost identical slopes near the Fermi energy for almost all elemental metals. As obtained from Landau Fermi liquid theory, the expressions for the band mass in LDA and  $G_0W_0$ , are [1, 52]

$$\frac{1}{m_{LDA}} = \frac{1}{m} + \frac{\partial V_{xc}}{\partial k} \times \frac{1}{k_F} \quad (1)$$

$$\frac{1}{m_{GW}} = Z \left( \frac{1}{m} + \frac{\partial \Sigma}{\partial k} \times \frac{1}{k_F} \right) \quad (2)$$

where  $V_{xc}$  and  $\Sigma$  are the exchange-correlation energy and GW self-energy respectively, while  $m$  is the bare electron mass,  $k_F$  is the Fermi wavevector, and  $Z$  is the renormalization factor. Since most of the metals studied here have very similar bandwidths, we can infer from the above equations that the changes coming from  $Z$  and  $\partial \Sigma / \partial k$ , which usually have opposite signs, cancel each other to give similar slopes in LDA and GW near the Fermi energy.

In DFT+eDMFT the mass is renormalized only by  $Z$ , as the self-energy has no momentum dependence. Hence, the cancellation between the momentum and frequency derivative does not occur, and the band narrowing is stronger. Given the much better agreement of eDMFT with the ARPES, this would suggest that the momentum dependence of the self-energy in this moderately correlated regime might be overestimated by GW, and that a better non-perturbative treatment of correlation effects should increase the frequency dependence and reduce the momentum dependence of the self-energy. Based on our study, however, we cannot exclude the possibility that the conventional interpretation of the ARPES experiments is invalid, and that the experimental narrowing of the bands is an artifact of final-state interactions [20] or surface effects [10, 28], opening up new possibilities and challenges for ARPES experiments in future.

*Conclusions:* For more than three decades, the electronic structure of elemental metals has been a subject of controversy. While they were assumed to closely approximate the uniform electron gas, the experimentally measured bandwidths were too narrow to fit this picture. Here, we have systematically studied the electronic structure of elemental metals from the first and second columns of the periodic table using LDA and various beyond-DFT methods, such as the mBJ meta-GGA and B3LYP hybrid functionals, GW, and DFT+DMFT (eDMFT), and compared with ARPES experiments where available. We have found that B3LYP significantly overestimates the bandwidths, even compared to LDA and mBJ, which are close to each other.  $G_0W_0$  reduces the bandwidths further, but still not sufficient, while eDMFT narrows the bands the most, producing spectral functions that match rather well with the ARPES experiments. These trends were found to follow almost uniformly over the elemental metallic family of compounds studied here.

Our study suggests that the elemental metals with partially occupied *s* orbitals are better described in terms of short-range dynamical correlations (local to an atom rather than to a point in 3D space) with predominantly large momentum unklapp contributions than in the weakly interacting perturbative picture, or in non-local hybrid schemes that incorporate purely local correlations and non-local Hartree-Fock exchange. Such a short-range dynamical description was already very successful for strongly correlated systems with partially filled *d* or *f* bands. Here, we conclude that it is also remarkably successful in describing moderately correlated simple metals as well.

## ACKNOWLEDGMENT

This research was funded by NSF DMREF DMR-1629059 and NSF DMREF DMR-1629346. The compu-

tations were performed at the Frontera supercomputer at the Texas Advanced Computing Center (TACC) at The University of Texas at Austin, which is supported by National Science Foundation grant number OAC-1818253 and at the Extreme Science and Engineering Discovery Environment (XSEDE), which is supported by National Science Foundation grant number ACI-1548562.

---

[1] G. D. Mahan, *Many-particle physics* (Plenum Press, New York, 1981).

[2] I.-W. Lyo and E. W. Plummer, *Phys. Rev. Lett.* **60**, 1558 (1988).

[3] E. Jensen, R. A. Bartynski, T. Gustafsson, E. W. Plummer, M. Y. Chou, M. L. Cohen, and G. B. Hoflund, *Phys. Rev. B* **30**, 5500 (1984).

[4] R. A. Bartynski, R. H. Gaylord, T. Gustafsson, and E. W. Plummer, *Phys. Rev. B* **33**, 3644 (1986).

[5] B. S. Itchkawitz, I.-W. Lyo, and E. W. Plummer, *Phys. Rev. B* **41**, 8075 (1990).

[6] V. A. Sashin, M. A. Bolorizadeh, A. S. Kheifets, and M. J. Ford, *Journal of Physics: Condensed Matter* **12**, 9407 (2000).

[7] M.-L. Shek, J. Hrbek, T. K. Sham, and G.-Q. Xu, *Phys. Rev. B* **41**, 3447 (1990).

[8] S. F. Elatresh, M. T. Hossain, T. Bhowmick, A. D. Grockowiak, W. Cai, W. A. Coniglio, S. W. Tozer, N. W. Ashcroft, S. A. Bonev, S. Deemyad, and R. Hoffmann, *Phys. Rev. B* **101**, 220103 (2020).

[9] G. D. Mahan and B. E. Sernelius, *Phys. Rev. Lett.* **62**, 2718 (1989).

[10] K. W. K. Shung, B. E. Sernelius, and G. D. Mahan, *Phys. Rev. B* **36**, 4499 (1987).

[11] W. Ku, A. G. Eguiluz, and E. W. Plummer, *Phys. Rev. Lett.* **85**, 2410 (2000).

[12] M. Vogt, R. Zimmermann, and R. J. Needs, *Phys. Rev. B* **69**, 045113 (2004).

[13] R. Maezono, M. D. Towler, Y. Lee, and R. J. Needs, *Phys. Rev. B* **68**, 165103 (2003).

[14] M. Higuchi, S. Yoshinaga, and H. Yasuhara, *Journal of the Physical Society of Japan* **68**, 3473 (1999), <https://doi.org/10.1143/JPSJ.68.3473>.

[15] L. Craco and S. Leoni, *Phys. Rev. B* **100**, 115156 (2019).

[16] F. Nilsson, L. Boehnke, P. Werner, and F. Aryasetiawan, *Phys. Rev. Materials* **1**, 043803 (2017).

[17] A. L. Kutzepov, *Phys. Rev. B* **94**, 155101 (2016).

[18] J. E. Northrup, M. S. Hybertsen, and S. G. Louie, *Phys. Rev. B* **39**, 8198 (1989).

[19] J. Lischner, T. Bazhirov, A. H. MacDonald, M. L. Cohen, and S. G. Louie, *Phys. Rev. B* **89**, 081108 (2014).

[20] H. Yasuhara, S. Yoshinaga, and M. Higuchi, *Phys. Rev. Lett.* **83**, 3250 (1999).

[21] H. Yasuhara, S. Yoshinaga, and M. Higuchi, *Phys. Rev. Lett.* **85**, 2411 (2000).

[22] L. Hedin, *Physical Review* **139**, A796 (1965).

[23] M. Higuchi, S. Yoshinaga, and H. Yasuhara, *Journal of the Physical Society of Japan* **68**, 3473 (1999), <https://doi.org/10.1143/JPSJ.68.3473>.

[24] G. Onida, L. Reining, and A. Rubio, *Rev. Mod. Phys.* **74**, 601 (2002).

[25] M. Holzmann, B. Bernu, C. Pierleoni, J. McMinis, D. M. Ceperley, V. Olevano, and L. Delle Site, *Phys. Rev. Lett.* **107**, 110402 (2011).

[26] R. Maezono, M. D. Towler, Y. Lee, and R. J. Needs, *Phys. Rev. B* **68**, 165103 (2003).

[27] X. Zhu and A. W. Overhauser, *Phys. Rev. B* **33**, 925 (1986).

[28] K. W. K. Shung and G. D. Mahan, *Phys. Rev. Lett.* **57**, 1076 (1986).

[29] A. Damascelli, Z. Hussain, and Z.-X. Shen, *Rev. Mod. Phys.* **75**, 473 (2003).

[30] G. Kotliar and D. Vollhardt, *Physics Today* **57**, 53 (2004).

[31] A. Georges, G. Kotliar, W. Krauth, and M. J. Rozenberg, *Rev. Mod. Phys.* **68**, 13 (1996).

[32] G. Kotliar, S. Y. Savrasov, K. Haule, V. S. Oudovenko, O. Parcollet, and C. A. Marianetti, *Rev. Mod. Phys.* **78**, 865 (2006).

[33] S. Biermann, A. Poteryaev, A. I. Lichtenstein, and A. Georges, *Phys. Rev. Lett.* **94**, 026404 (2005).

[34] J. Kuneš, A. Yamasaki, A. V. Lukyanov, M. Feldbacher, V. I. Anisimov, Y. F. Yang, R. T. Scalettar, O. Andersen, W. E. Pickett, and K. Held, *Nature Mat.* **7**, 198 (2008).

[35] H. Park, A. J. Millis, and C. A. Marianetti, *Phys. Rev. Lett.* **109**, 156402 (2012).

[36] P. R. C. Kent and G. Kotliar, *Science* **361**, 348 (2018).

[37] E. Gull, A. J. Millis, A. I. Lichtenstein, A. N. Rubtsov, M. Troyer, and P. Werner, *Rev. Mod. Phys.* **83**, 349 (2011).

[38] J. H. Shim, K. Haule, and G. Kotliar, *Nature* **446**, 513 (2007).

[39] Z. P. Yin, K. Haule, and G. Kotliar, *Nat. Mater.* **10**, 932 (2011).

[40] S. Mandal, P. Zhang, S. Ismail-Beigi, and K. Haule, *Phys. Rev. Lett.* **119**, 067004 (2017).

[41] J. Ferber, K. Foyevtsova, R. Valentí, and H. O. Jeschke, *Phys. Rev. B* **85**, 094505 (2012).

[42] P. Blaha, K. Schwarz, G. Madsen, D. Kvasnicka, and J. Luitz, “An augmented plane wave plus local orbitals program for calculating crystal properties,” (Vienna University of Technology, Austria, 2001, 2001).

[43] K. Haule and S. Mandal, arXiv:2008.07727 (2020).

[44] I.-W. Lyo and E. W. Plummer, *Phys. Rev. Lett.* **60**, 1558 (1988).

[45] F. Tran, P. Blaha, K. Schwarz, and P. Novák, *Phys. Rev. B* **74**, 155108 (2006).

[46] J. Heyd, G. E. Scuseria, and M. Ernzerhof, *The Journal of Chemical Physics* **118**, 8207 (2003).

[47] J. P. Perdew, M. Ernzerhof, and K. Burke, *The Journal of Chemical Physics* **105**, 9982 (1996).

[48] C. Lee, W. Yang, and R. G. Parr, *Phys. Rev. B* **37**, 785 (1988).

[49] S. Mandal, K. Haule, K. M. Rabe, and D. Vanderbilt, *npj Computational Materials* **5**, 115 (2019).

[50] J. Paier, M. Marsman, and G. Kresse, *The Journal of Chemical Physics* **127**, 024103 (2007), <https://doi.org/10.1063/1.2747249>.

[51] A. Kutzepov, V. Oudovenko, and G. Kotliar, *Computer Physics Communications* **219**, 407 (2017).

[52] K. Haule and K. Chen, arXiv:2012.03146 (2020).

[53] F. Tran and P. Blaha, *Phys. Rev. Lett.* **102**, 226401 (2009).

[54] A. D. Becke, *The Journal of Chemical Physics* **98**, 5648 (1993).

- [55] K. Haule, C.-H. Yee, and K. Kim, Phys. Rev. B **81**, 195107 (2010).
- [56] K. Haule, Journal of the Physical Society of Japan **87**, 041005 (2018), <https://doi.org/10.7566/JPSJ.87.041005>.
- [57] <http://hauleweb.rutgers.edu/tutorials>.
- [58] K. Haule, Physical Review B **75** (2007).
- [59] K. Haule, Phys. Rev. Lett. **115**, 196403 (2015).

## SUPPLEMENTAL MATERIAL

### COMPUTATIONAL DETAILS

In this work we have used the full potential linear augmented plane wave (LAPW) method as described in the WIEN2k [42] software for various DFT and beyond-DFT methods, such as the modified Becke-Johnson (mBJ) potential [53] for meta-GGA, B3LYP [45, 54] for hybrid functionals, all electron GW (PyGW software [43]) for Hedin's GW formalism, and embedded DMFT (eDMFT) [55, 56] method for dynamical mean field theory. For  $G_0W_0$ , mBJ and B3LYP we construct the initial wavefunction and eigenvalues with LDA functional.

**DFT+DMFT:** We have used a fully self-consistent DFT-DMFT code, developed at Rutgers by one of the co-authors [57], where the continuous-time quantum Monte Carlo method [58] is used to solve the quantum impurity problem that is embedded within the Dyson equation for the solid, to obtain the local self-energy for the metal's  $s$  orbitals. In this embedded-DMFT(eDMFT) method [55, 56] we use the LDA functional and the LAPW basis set as implemented in WIEN2k [42]. Using the *exact* double counting between LDA and DMFT [59], we obtain the self-energy on Matsubara frequency which is then analytically continued with the maximum entropy method from the imaginary to the real axis, continuing the local cumulant function, to obtain the partial density of states and then the spectral functions. In eDMFT, where all such higher-order Feynman diagrams are explicitly calculated by the impurity solver, the amount of screening by the degrees of freedom not included in the method is substantially reduced, and the values of  $U$  are larger and are quite successfully predicted by the self-consistent constrained method. A fine k-point mesh of at least  $15 \times 15 \times 15$  k-points in Monkhorst-Pack k-point grid and a total of 20 million Monte Carlo steps for each iteration are used for the elemental metals at  $T=300K$ . To avoid tuning parameters, the Coulomb interaction  $U$  and Hund's coupling  $J_H$  are fixed at 5.0 eV and 0.3 eV respectively. These values are computed by the constrained-eDMFT method. The computed values of

$U$  vary much weakly among the compounds than the change in the bandwidth with changing  $U$ . Hence we fix

Compound ICSD-ID

Compound	ICSD-ID
Li	44367
Be	1425
Na	196972
Mg	76748
K	44670
Ca	44348
Rb	44869
Sr	76162
Cs	42662
Ba	96587

TABLE S1. ICSD-IDs for compounds studied here.

$U = 5.0$  eV for all elemental metals studied here. The  $U$ -dependence spectral function is shown in Fig. S1. for Na.

**GW:** We perform single-shot GW ( $G_0W_0$ ) using PyGW software package [43], an all-electron GW software, where GW self-energy is computed within the all-electron LAPW basis of WIEN2K. In this newly developed GW code, special attention is paid to the metallic systems and proper treatment of deep laying core states. We carefully converge our results using a very fine k-point mesh as the convergence for metallic systems can be a point of difficulty in GW computation. Here, even though we use tetrahedron analytic integration over momentum points, we find that a large number of momentum points is necessary for convergence. For example, a  $4 \times 4 \times 4$  grid although gives approximate spectra not too different from LDA, the convergence reaches only at  $16 \times 16 \times 16$  momentum mesh. For more details about methodology and K-point convergence, we refer the reader to Ref. [43].

## CRYSTAL STRUCTURES

The experimental crystal structures are obtained from the ICSD-database. The ICSD numbers are given in Table S1.

## RESULTS

In Figs. S2-S3, we describe band structures for elemental Be, Sr, Cs, Ca, and Rb as computed in LDA, mBJ,  $G_0W_0$ , B3LYP, and eDMFT in various energy windows.

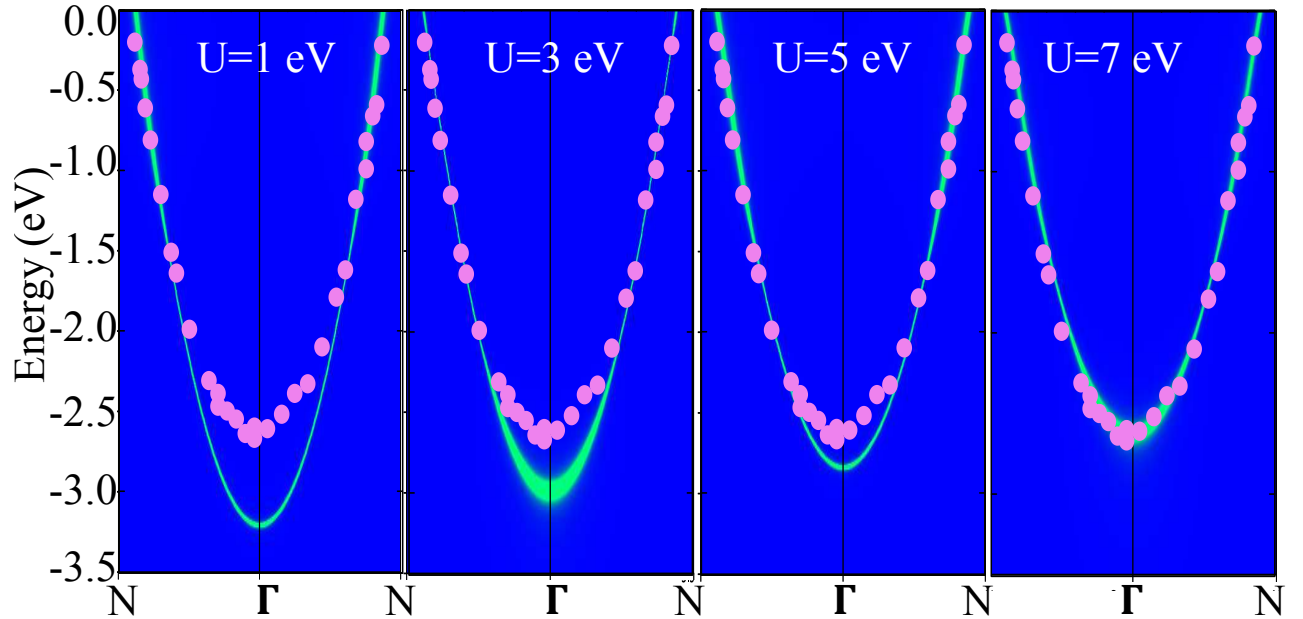


FIG. S1. (Color online) The dependence of Coulomb  $U$  in eDMFT spectral function for elemental Na. Pink dots indicate angle-resolved-photoemission(ARPES) data from Ref. [2].

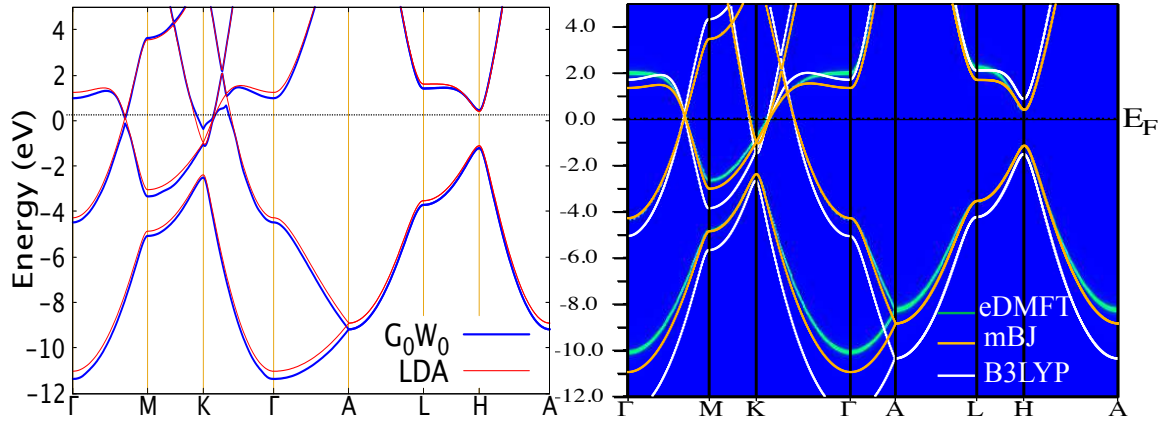
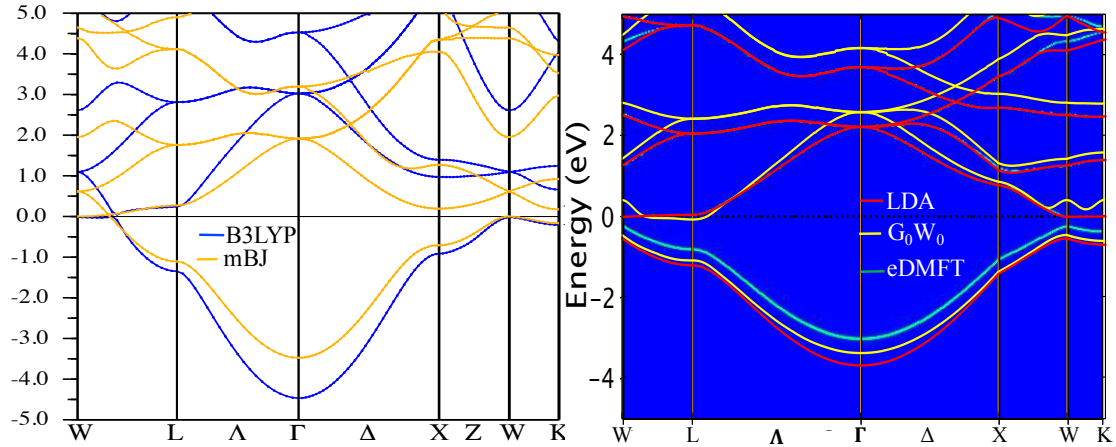
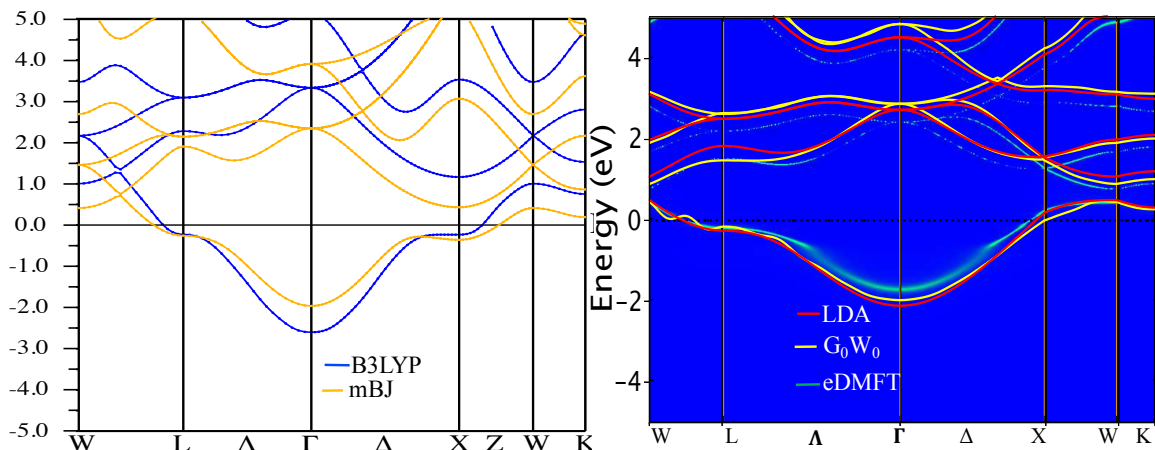
**Be****Sr****Cs**

FIG. S2. (Color online) Band structures of elemental Be (top), Sr (middle) and Cs (bottom) as computed in LDA, mBJ,  $G_0W_0$ , B3LYP, and eDMFT.

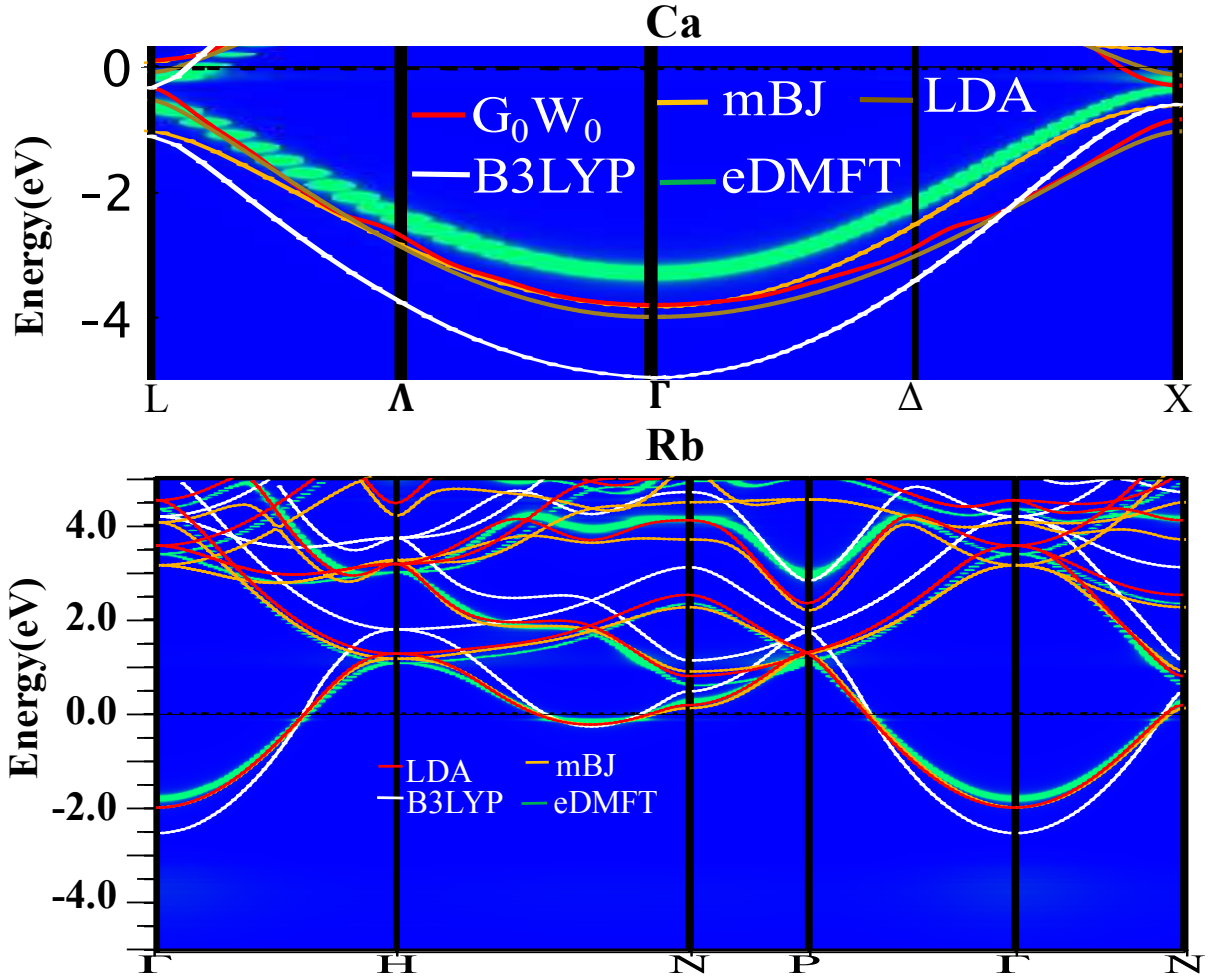


FIG. S3. (Color online) Band structures of elemental Ca (top) and Rb (bottom) as computed in LDA, mBJ,  $G_0W_0$ , B3LYP, and eDMFT.